Neutron-diffraction investigation of structural changes during inverse melting of $Ti_{45}Cr_{55}$

W. Sinkler,* C. Michaelsen, and R. Bormann
GKSS Research Center, Institute for Materials Research, 21502 Geesthacht, Germany

D. Spilsbury and N. Cowlam
Department of Physics, University of Sheffield, Sheffield, S3 7RH, United Kingdom
(Received 2 August 1996)

The inverse-melted amorphous phase of $Ti_{45}Cr_{55}$, as well as the precursor bcc phase has been investigated using neutron scattering. An increase in chemical short-range order (CSRO), which involves primarily a differentiation of Ti and Cr sites in the alloy is detected, in line with expectations based on a decrease in the entropy which accompanies the crystalline to amorphous (c-to-a) transformation. The CSRO in the amorphous phase shows a weak preference for unlike neighbor pairs. The neutron data indicate that similarities exist between the local structure of the inverse melted amorphous phase and the $TiCr_2$ Laves compound. These similarities are indicative of topological medium-range order (MRO) in the amorphous phase which resembles that of the Laves compound. [S0163-1829(97)03105-6]

I. INTRODUCTION

Inverse melting transformations have recently been reported in a number of binary bcc alloys based on the early transition metals Ti, Nb, Zr, and Ta with later transition metals from groups V or VI.[1–4] In inverse melting, a metastable supersaturated alloy transforms polymorphously to the amorphous, or undercooled liquid state. This transformation is thus like melting, except that the resulting phase is the undercooled liquid or an amorphous phase near the glass temperature (T_g), as opposed to the high-temperature equilibrium melt. In contrast to normal melting, which is an endothermic transformation, inverse melting is exothermic and results in a phase which has both a lower entropy S as well as lower enthalpy H than the crystalline precursor.[5] Figure 1 shows a metastable phase diagram of the Ti-Cr system,[1] calculated using the Calphad method.[6] In the diagram, only bcc, liquid ($T>T_g$), and amorphous phases ($T<T_g$) are considered. As can be seen, the high-temperature liquid and low-temperature amorphous phase fields are separated by a region of complete solid miscibility in the bcc phase. Based on the occurrence of a congruent amorphous to bcc transformation in metastable equilibrium at 55 at. % Cr and 746 °C, the low-temperature amorphous phase must have both a lower entropy as well as a lower enthalpy than the bcc phase.

The existence of a low-temperature amorphous phase field in Fig. 1 indicates that if the bcc phase can be obtained at low temperature within the amorphous phase field, it will be unstable with respect to the amorphous phase, and can thus transform to the amorphous phase. Using ball milling in a planetary mill, homogeneous bcc phases have been produced at compositions $0.4 \leqslant x_{Cr} \leqslant 0.65$ in the Ti-Cr system.[1] Alloys with 55 at. % Cr were found to undergo a polymorphous c-to-a transformation on heat treatment,[1] in agreement with the predictions of the metastable phase diagram.

These results raise two fundamental questions: The first is how the amorphous phase can have a lower entropy than the crystalline bcc phase. This is surprising from a structural point of view, because the crystal is topologically long-range ordered, whereas the amorphous phase is not and thus might be expected to have the higher entropy. The second question is why the bcc phase is actually formed in the ball mill, in spite of the fact that the Gibbs energy of the amorphous phase is lower (see Fig. 1). A unified answer to both these questions has been proposed[7,8] which is based on differing degrees of chemical short-range order (CSRO) in the bcc and amorphous phases. In concentrated Ti-Cr alloys it is found that processing which tends to strongly disorder, including both ball milling and also low-temperature ion[9–11] and electron[12] irradiation, lead to formation of a bcc phase. This suggests that the relative stability of bcc and amorphous phases is sensitive to the degree of CSRO, with the bcc phase being more stable than amorphous when the degree of CSRO is small. Only when the CSRO is allowed to increase to its equilibrium value for both bcc and amorphous phases does the amorphous phase become more stable than the bcc phase, as reflected in the metastable phase diagram.

These considerations are illustrated in Fig. 2, which is a schematic plot of the Gibbs energies of the bcc and amorphous phases versus a CSRO parameter η. The plot explains schematically how the relative stability depends on the processing conditions, which may be varied to produce either the bcc or amorphous phase. The validity of the plot is sup-

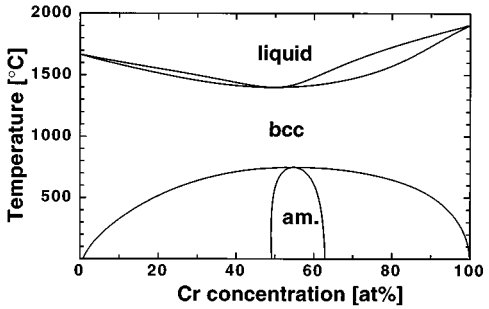

FIG. 1. Metastable phase diagram for the Ti-Cr system (Ref. 1).

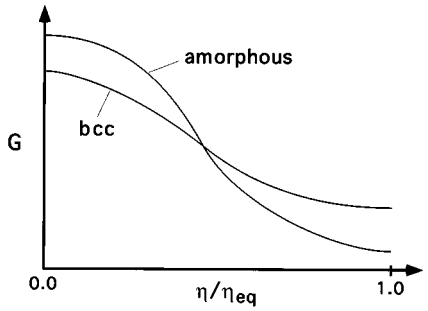

FIG. 2. Schematic plot of the Gibbs energy vs a CSRO parameter η for systems exhibiting inverse melting. η_{eq} is the (metastable) equilibrium value of η for the phase in question. At low η, the bcc phase is more stable than the amorphous phase, as demonstrated by irradiation and ball-milling experiments. When short-range order is allowed to develop, as in annealing experiments, the amorphous phase becomes more stable due to the stronger dependence of the amorphous free energy on CSRO than is the case for the bcc phase. This permits the occurrence of a *c*-to-*a* transformation.

ported by the fact that the amorphous phase produced by inverse melting can be remilled to again form a bcc phase.[13] The plot also explains why alloys which form $B2$ phases generally do not undergo inverse melting.[8] In the case of $B2$ ordering, the chemical order may increase without a topological deviation from the bcc lattice. Clearly, a substantial energy reduction, which occurs effectively within the bcc phase, would reduce the energy available for transformation to the amorphous state. Thus the possibility of substantially reducing the energy within the bcc phase, for instance, via a $B2$-like CSRO would result in the absence of a crossing point of the Gibbs energy curves of the bcc and amorphous phases in Fig. 2. This indicates that CSRO on the bcc lattice must be limited,[14] and that energy reduction via CSRO must be coupled with substantial strain from the bcc topology, in alloys which undergo inverse melting.

The possibility of pronounced CSRO lending stability to the amorphous phase is supported by previous studies which confirm that amorphous metallic alloys often exhibit CSRO.[15–17] Nevertheless, while the argument based on CSRO is convincing and explains the observed transformations well, it has to date lacked direct experimental verification. Near-equiatomic alloys of Ti-Cr offer a unique opportunity for measuring CSRO using neutron scattering, because their average scattering length for neutrons is very small. Because of this, neutron diffraction is particularly sensitive to CSRO at the $Ti_{45}Cr_{55}$ alloy composition, for which the polymorphous *c*-to-*a* transformation is observed. This has been utilized previously to study CSRO in bulk-quenched and annealed Ti-Cr alloys.[18] An additional motivation for the study is simply to provide sensitive structural information concerning an amorphous phase produced by inverse melting, in order to determine how it compares structurally to other amorphous metals. In the present work, ball-milled and subsequently heat treated $Ti_{45}Cr_{55}$ alloys have been investigated using diffuse neutron scattering, in order to provide structural information and to measure the development of CSRO in the course of inverse melting.

II. NEUTRON-DIFFRACTION THEORY

In a neutron-scattering experiment the coherently scattered intensity per atom $I_{coh}(Q)$ for a binary alloy is related to the total structure factor $S(Q)$ as $I_{coh}(Q)=\langle b^2\rangle S(Q)$, where $\langle b^2\rangle$ is the mean-square nuclear scattering length. According to the work of Bhatia and Thornton,[19] the total $S(Q)$ may be split into three partial structure factors. This results in

$$I_{coh}(Q)=\langle b\rangle^2 S_{NN}(Q)+(b_1-b_2)^2 S_{CC}(Q)+2\langle b\rangle(b_1-b_2)S_{NC}(Q), \tag{1}$$

where b_i is the neutron-scattering length of element i, $S_{NN}(Q)$ is a partial structure factor related to spatial fluctuations in the number density of the atoms, regardless of species, $S_{CC}(Q)$ is related to fluctuations in the distributions of the two chemical species in the alloy, and $S_{NC}(Q)$ is related to correlations between number density and chemical distribution fluctuations. From Eq. (1), the weighting factors for the contributions of the partial structure factors to the total $S(Q)$ are

$$\omega_{NN}=\frac{\langle b\rangle^2}{\langle b^2\rangle},\quad \omega_{CC}=\frac{(b_1-b_2)^2}{\langle b^2\rangle},\quad \text{and}$$

$$\omega_{NC}=\frac{2\langle b\rangle(b_1-b_2)}{\langle b^2\rangle}. \tag{2}$$

For a $Ti_{45}Cr_{55}$ alloy, using Ti as component 1 and Cr as component 2 results in $\omega_{NN}=0.0163$, $\omega_{CC}=3.9745$, and $\omega_{NC}=-0.5057$. Using expressions for the partial structure factors from Bhatia and Thornton,[19] one obtains the reduced radial distribution function $G(r)$ as

$$\begin{aligned}G(r)=4\pi\rho_0 r\{&(\omega_{NN}x_1^2+\omega_{CC}x_1^2x_2^2+\omega_{NC}x_1^2x_2)P_{11}(r)\\&+(\omega_{NN}x_2^2+\omega_{CC}x_1^2x_2^2-\omega_{NC}x_1x_2^2)P_{22}(r)\\&+[2\omega_{NN}x_1x_2-2\omega_{CC}x_1^2x_2^2\\&+\omega_{NC}x_1x_2(x_2-x_1)]P_{12}(r)-\omega_{NN}\}\end{aligned} \tag{3}$$

in which ρ_0 is the number density of atoms in the sample, x_1 and x_2 are the atomic fractions of Ti and Cr, respectively, and $P_{\alpha\beta}(r)$ is a pair probability for α-β pairs at a distance r, normalized to equal one at large r.

In the case of a binary solid solution with a simple structure such as bcc, neighbor shells can be defined which are topologically the same for both elements in the sample. In this case, the Cowley-Warren short-range order parameter, α,[20] can be obtained directly from $G(r)$, except when $b_1\approx b_2$. Averaged over the atoms of the pth coordination shell, α is given by

$$\alpha_p=1-\frac{N_{21}}{x_2 n_p}, \tag{4}$$

in which N_{21} is the number of 2 atoms in the pth shell around central 1 atoms, averaged over all 1 atoms in the sample, and n_p is the total number of atoms in the pth neighbor shell. If one considers that the average number of atoms of type α in the pth shell around central β atoms is

$$N_{\alpha\beta}=\int_{p\text{th shell}} 4\pi r^2 \rho_0 x_\alpha P_{\alpha\beta}(r)dr. \tag{5}$$

Then, using $P_{12}(r)=P_{21}(r)$ and $N_{12}=(x_1/x_2)N_{21}$ one finds from Eqs. (3)–(5)

$$\frac{1}{n_p}\int_{p\text{th shell}} r[G(r)+\omega_{NN}4\pi\rho_0 r]dr$$

$$=\alpha_p(\omega_{CC}x_1x_2+2\omega_{NC}x_1^2x_2)+\omega_{NN}. \tag{6}$$

This allows α_p to be determined directly from an experimental $G(r)$ when ω_{CC} is sufficiently large, as in the present case.

In binary amorphous alloys, the coordinations of the two atom types are in general different. Because of this, a single parameter is not sufficient to fully describe the state of chemical order. Equation (5) is nevertheless still valid for a given range of r, and one can combine this with Eq. (3) to obtain

$$\int_r^{r+\Delta r} r(G(r)+\omega_{NN}4\pi\rho_0 r)dr$$

$$=(\omega_{NN}x_1+\omega_{CC}x_1x_2^2+\omega_{NC}x_1x_2)N_{11}$$
$$+(\omega_{NN}x_2+\omega_{CC}x_1^2x_2-\omega_{NC}x_1x_2)N_{22}$$
$$+[2\omega_{NN}x_2-2\omega_{CC}x_1x_2^2+\omega_{NC}x_2(x_2-x_1)]N_{12}. \tag{7}$$

If one can isolate ranges of r in which only one of the N's is significant, for instance, based on bond lengths, one can use Eq. (7) to determine local coordinations in the alloy. In the present case, using Ti as element 1 and Cr as element 2, the coefficients of the $N_{\alpha\beta}$ on the right-hand side of Eq. (7) are 0.4232 (for N_{11}), 0.5768 (for N_{22}), and -1.0773 (for N_{12}). The atomic number density is 69.8 nm^{-3}, based on the bcc lattice parameter (see below).

III. EXPERIMENT

Two batches of bcc $Ti_{45}Cr_{45}$ powder were produced by ball milling. In the first batch, mechanical alloying (MA) of elemental Ti and Cr powders was used. For the second batch, bulk materials were prealloyed in an arc melter, and subsequently crushed to a powder in an argon glove box using a steel mortar prior to mechanical milling (MM). Details on the milling of both MA and MM powders are described in Ref. 1. Milling times were 150 h for the MA powder and 90 h for the MM powder. Energy dispersive x-ray-spectroscopy measurements in a scanning electron microscope indicated that the MA powder contained less than 0.2 at. % Fe, and the MM powder less than 1.9 at. % Fe. Analysis of gaseous impurities for the final MM powder showed 900 wt. ppm O and 650 wt. ppm N.

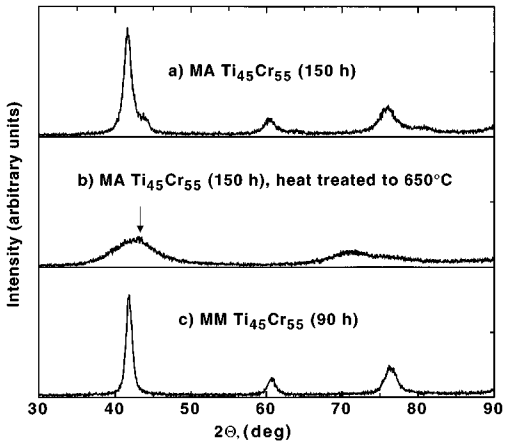

FIG. 3. CuK_α x-ray-diffractometer traces for MA and MM $Ti_{45}Cr_{55}$ (traces *a* and *c*), as well as inverse melted $Ti_{45}Cr_{55}$ (trace *b*). The arrow in *b* points to a small (113) C15 reflection, which is just visible superimposed on the first amorphous halo. The powder for trace *b* was produced by heating the trace *a* powder to a temperature of 650 °C in a calorimeter at 20 K/min.

A heat treatment of the MA powder was performed in order to produce the amorphous phase. The powder was heated at 20 K/min to 650 °C in a Netzsch DSC 404 calorimeter under flowing argon (99.9999% argon). Impurity analysis of the amorphous phase indicated 2200 wt. ppm O and 730 wt. ppm N.

Figure 3 shows CuK_0 x-ray diffractometer traces of the milled nanocrystalline bcc MA (trace *a*) and MM (trace *c*) powders, as well as of the amorphized MA powder (trace *b*). The as-milled MA powder still contains some undissolved Cr after 150 h milling, which is seen as a high-angle shoulder on the main (110) diffraction peak. However, after this much milling time, the Cr grain size should be about 20 nm or less, and the grains are embedded in a substantially homogeneous Ti-Cr alloy. As Ti and Cr have been found to react in thin film experiments to produce an amorphous phase,[21] the Cr inhomogeneities should be reduced in the course of the *c*-to-*a* transformation. This is supported by the absence of any detectable Cr peaks in trace *b*) of Fig. 3. The lattice parameters of the bcc phases of MA and MM powders are 0.3070 nm and 0.3052 nm, respectively. Based on the closely linear lattice parameter versus composition behavior in the Ti-Cr bcc phase,[1,22] one may use the lattice parameters to obtain a rough estimate of the compositions of the two bcc alloys. This indicates compositions of approximately 53 at. % Cr and 57 at. % Cr, in support of a small degree of inhomogeneity in the MA alloy.

The x-ray-diffraction trace of the amorphous phase produced after heat treating the MA powder to 650 °C in the DSC shows a substantial decrease in coherent scattering, with the sharp diffraction spots of the bcc phase being replaced by broad features typical of an amorphous phase. Nevertheless, a small quantity of the $TiCr_2$ Laves compound was produced during the anneal, as is indicated by the small peak corresponding to (311) of the C15 $TiCr_2$ Laves compound (arrow in Fig. 3). This contrasts with the results of Yan *et al.*,[1] and is possibly explained by the presence of Cr-rich regions in the starting bcc powder in the present case.

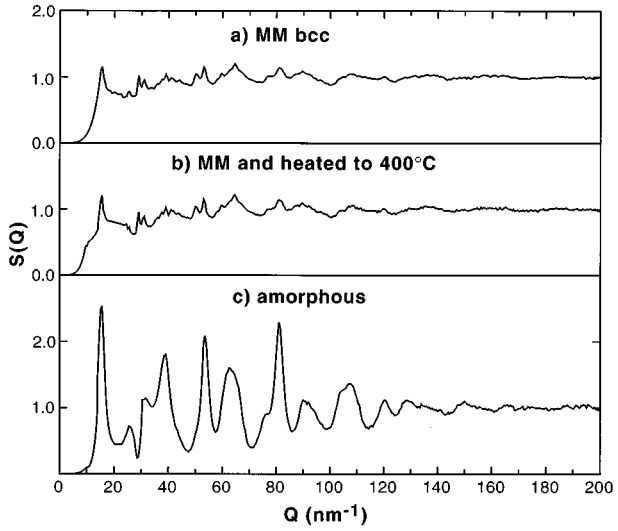

FIG. 4. Experimental $S(Q)$'s for the MM $Ti_{45}Cr_{55}$ (trace *a*), the same heated briefly to 350 °C (trace *b*), and the inverse melted amorphous $Ti_{45}Cr_{55}$ (trace *c*).

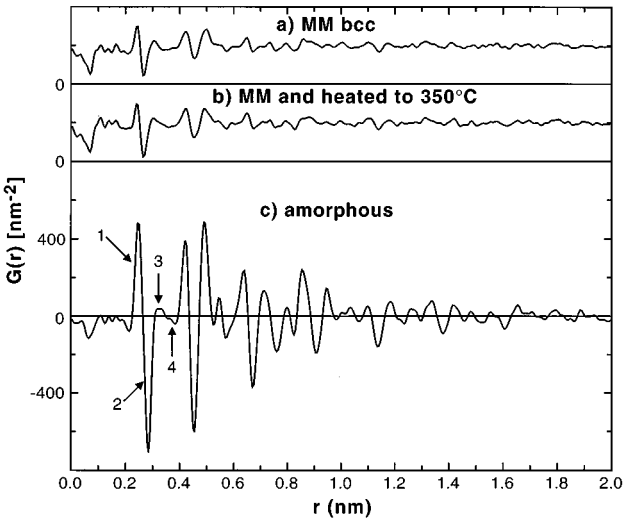

FIG. 5. $G(r)$ corresponding to the $S(Q)$'s in Fig. 4. The first four peaks in $G(r)$ for the amorphous phase are labeled as in Table I.

A further check of the amorphous alloy was performed using TEM. The results of bright and dark field imaging are similar to those presented elsewhere for inverse melted $Ti_{50}Cr_{50}$ (Ref. 1) and $Nb_{45}Cr_{55}$ (Ref. 23) alloys, and are consistent with the presence of an amorphous phase plus a small minority component of the Laves compound.

The two Ti-Cr powders, amorphous and MM were investigated using time-of-flight diffuse neutron scattering on the liquid and amorphous diffractometer (LAD) at Rutherford Appleton Laboratory, Chilton, UK. A third neutron measurement was subsequently made of the MM powder, after a brief ($\approx$10 min *ex situ* heating of this powder to a temperature of 350 °C in the vanadium can used for neutron measurement. This measurement was performed in order to determine what changes in CSRO occur during low-temperature annealing of the bcc phase prior to the inverse melting transformation. For neutron diffraction, each of the specimens weighed approximately 7 g. The measurements were made after evacuating the diffractometer to below 10^{-3} mbar to avoid air scattering. Instrumental details, including the reduction of the raw data to obtain $S(Q)$ and $G(r)$ are described in Refs. 24 and 25.

Plots of $S(Q)$ and $G(r)$ for the three samples are shown in Figs. 4 and 5. As is clearly seen, the peaks in both the $S(Q)$ and $G(r)$ for the amorphous case tend to be larger than in either the as-milled or annealed cases. Because the partial structure factor corresponding to chemical correlations, $S_{CC}(Q)$, is strongly weighted in this alloy, the neutron data are dominated by CSRO. It is important to note that for the particular alloy investigated about 98% of the scattering intensity originates from CSRO effects, whereas less than 2% is due to topological short-range ordering (TSRO). The large peaks for the amorphous phase compared to the relatively flat traces for the bcc alloy are thus primarily the signature of a strong increase in CSRO, in agreement with the predicted behavior as described in the Introduction. In the following two sections, the amorphous and the as-milled and annealed traces are analyzed in detail.

IV. ANALYSIS OF NEUTRON-DIFFRACTION DATA

A. Amorphous $Ti_{45}Cr_{55}$

The amorphous $G(r)$ was analyzed using Eq. (7). The small term $\omega_{NN}\times 4\pi\rho_0 r$ was added to the experimental $G(r)$. This was then multiplied by r and the integrals were taken over intervals corresponding to the peaks in $G(r)$. The results of the integration for the first four peaks in $r\times G(r)$ are shown in Table I.

The mean distance of peak 1 is 0.245 nm. This compares closely with the Cr-Cr nearest-neighbor distance in pure Cr (0.249 nm), and matches exactly the Cr-Cr nearest-neighbor distance in the $TiCr_2$ Laves compound.[26] It is also significantly smaller than either the Ti-Cr nearest-neighbor distance for $TiCr_2$ (0.285 nm) or typical Ti-Ti nearest-neighbor distances of 0.295–0.306 nm for α-Ti and $TiCr_2$, respectively. Based on the fact that the first peak ends at 0.265 nm it should not include either Ti-Cr or Ti-Ti pairs. From Eq. 7 the first peak integral is thus equal to $0.5768\times N_{\mathrm{CrCr}}$ for this interval. This indicates that Cr atoms are coordinated by an average of 4.81 Cr atoms at a distance of 0.245 nm.

In the present $G(r)$, the distance corresponding to peaks 2 through 4 covers the Ti-Cr and Ti-Ti nearest-neighbor distances for the $TiCr_2$ compound, without including any contribution from the second-neighbor shell. The latter begins at 0.425 nm in $TiCr_2$ and 0.432 nm in the bcc precursor phase, suggesting that peaks beyond 0.395 nm belong to second- or higher-neighbor shells in the present data. The evaluation of peaks 2–4 is nevertheless complicated in the present case by

TABLE I. Analysis of $G(r)$, amorphous phase.

Peak	r limits (nm)	$\int r(\mathrm{G(r)}+\omega_{\mathrm{NN}}4\pi\rho_0\mathrm{r})\mathrm{dr}$
1	0.225–0.265	2.776
2	0.265–0.310	−4.784
3	0.310–0.350	0.427
4	0.350–0.395	−0.277

the fact that none of the $N_{\alpha\beta}$ can be assumed to equal zero in this interval. The total coordination number of Cr, N_{Cr}, can be written

$$N_{\mathrm{Cr}}=4.81+X+N_{\mathrm{TiCr}}. \tag{8}$$

Here, 4.81 is N_{CrCr} for $r<0.265$ nm, as deduced from peak 1, X represents N_{CrCr} for the range $0.265<r<0.395$ nm, and N_{TiCr} is the number of Ti atoms in the first coordination shell of Cr. From Table I, the left-hand side of Eq. (7) for r over the range of peaks 2–4 is -4.634. Using Eq. (7) for this range, making a substitution for N_{TiCr} from Eq. (8), and setting $\Delta N=N_{\mathrm{Ti}}$-N_{Cr} as the difference in coordination numbers between Ti and Cr, one can rearrange Eq. (7) to obtain an equation of the form

$$N_{\mathrm{Cr}}=A+B\Delta N+CX. \tag{9}$$

By inserting numerical values for all parameters in Eq. (7) one obtains $A=10.50$, $B=0.361$, and $C=1.85$. Although it is not possible to conclusively determine the first-neighbor coordinations from this equation with three unknowns, the uncertainty can be reduced by the following considerations: Cr is smaller than Ti, and ordering in the Ti-Cr system should thus tend to reduce the coordination number of Cr from 14 as in bcc toward a minimum value of 12 which is realized in the $TiCr_2$ compound. Based on this, N_{Cr} is confined between 12 and 14. Similarly, for the case of Ti the maximum possible coordination number is 16. This is the coordination number of Ti in the $TiCr_2$ Laves compound. In the compound, Ti has 12 Cr and 4 Ti nearest neighbors. Because the composition of the amorphous phase is Ti rich with respect to the $TiCr_2$ stoichiometry, it is likely that Ti has more Ti first neighbors in the present case than in $TiCr_2$. Considering that the first coordination shell of Ti in the Laves compound is close packed, and that Ti is larger than Cr, this would indicate a coordination number for Ti which is less than 16. As a preliminary assumption, one can set X equal to zero. This eliminates the unlikely scenario that a significant portion of the Cr-Cr nearest-neighbors pairs actually increases their distance in the transformation, with respect to the initial bcc Ti-Cr alloy's nearest-neighbor distance of 0.265 nm.

Based on these considerations N_{Cr} is closely confined to approximately 12. This is because if X is zero, setting $N_{\mathrm{Cr}}=12$ results in $\Delta N=4.1$ in Eq. (9), i.e., $N_{\mathrm{Ti}}=16.1$. Any increase in N_{Cr} simply forces ΔN to further increase, as long as $X=0$. This suggests that the average N_{Cr} for the first shell is very close to 12, while a small but finite X compensates ΔN in Eq. (9) to yield a Ti coordination number slightly less than 16. Assuming that X is in the range 0.03–0.3 allows the coordination of Cr to be assessed as a total coordination number of 12–12.4, of which 4.8–5.1 are Cr. The corresponding coordination numbers for Ti are a total coordination of 15.5 ± 0.5, of which 8.8–9 are Cr and the rest Ti.

In Fig. 6, the present experimental $G(r)$ for the amorphous phase is compared with a calculated $G(r)$ for the $TiCr_2$ Laves compound.[27] As can be seen, the curves are similar, and there is an apparent correspondence of the peaks up to $r\approx0.7$ nm. In the present assessment, the uncertainty of the coordination numbers is strongly dependent on the upper limit assumed for X. If X is confined to near zero, the coordination numbers can only vary within close tolerances, and

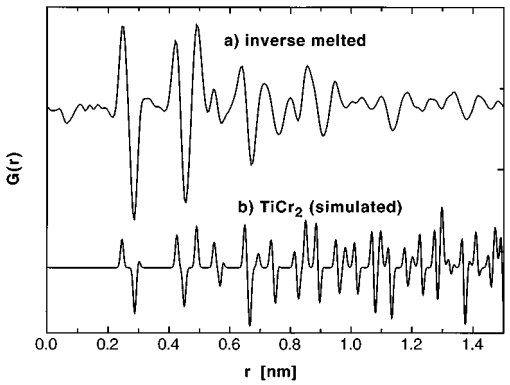

FIG. 6. Comparison of $G(r)$'s of inverse melted $Ti_{45}Cr_{55}$ (experimental, trace *a*) and a calculated trace for the $TiCr_2$ compound (trace *b*) (Ref. 27). Trace *b* was calculated using atom positions given by Duwez and Taylor (Ref. 26).

the numbers themselves are similar to those in the Laves compound. The overall similarity of the amorphous $G(r)$ and that calculated for the Laves compound in Fig. 6 suggests that the atomic coordinations in the present amorphous phase and the $TiCr_2$ Laves compound are indeed similar. This adds overall support for the assumption that X is at most 0.3, i.e., the average Cr atom has at most 0.3 Cr neighbors in the range $0.265<r<0.395$ nm.

Although the atomic coordinations in the amorphous phase are similar to those in the Laves compound, they are not identical. The first-neighbor shell value of 4.8 to 5.2 for N_{CrCr} is smaller than in the case of the Laves compound, in which Cr has 6 Cr nearest neighbors. This difference is consistent with the larger Ti concentration in the alloy than in stoichiometric $TiCr_2$, as this would tend to increase the number of Ti nearest neighbors of Cr. This can also explain why Ti has approximately 9 Cr nearest neighbors in the present assessment, compared to 12 in the $TiCr_2$ compound. The deviations in the first shell coordinations from those of the Laves compound would tend to result in internal strains of any regions with a Laves-like topology. While the local coordinations assessed here resemble those in the Laves compound, the CSRO deduced above cannot be merely a characteristic of a very small volume fraction of $TiCr_2$, such as that suggested by x-ray diffractometry (see Fig. 3, trace *b*). This is because Cr atoms in the Laves compound have six nearest-neighbor Cr atoms at 0.245 nm, whereas from the present results the *average* Cr atom in the inverse melted sample has 4.8 Cr neighbor atoms at this distance. The significance of the structural similarity between the amorphous phase and the Laves compound will be dealt with further in the Discussion.

B. As-milled and annealed bcc $Ti_{45}Cr_{55}$

The $S(Q)$ and $G(r)$ traces in the as-milled and annealed specimens are strikingly similar. In addition, the main features of the $G(r)$ curves do not correspond to the neighbor shells of the bcc phase. This is shown in Fig. 7, in which $G(r)$ for the as-milled specimen is also compared with a calculated $G(r)$ for the $TiCr_2$ Laves compound structure given by Duwez and Taylor.[26] The features of the as-milled $G(r)$ are consistent with the presence of the Laves com-

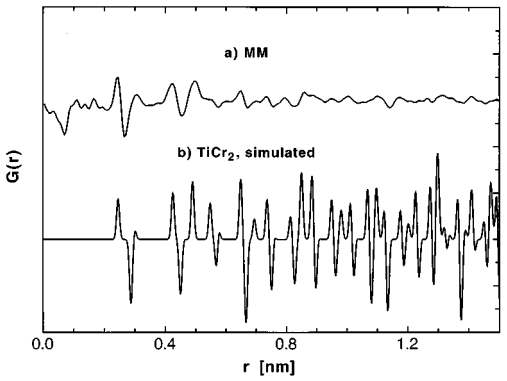

FIG. 7. Comparison of $G(r)$ for as-milled MM powder, and $TiCr_2$ (calculated) (Ref. 27).

pound in the sample, in spite of the bcc x-ray-diffraction trace shown in Fig. 3, trace c. This leads to the suspicion that the Laves phase produced on initial arc melting of the specimen was not fully transformed to bcc by milling. This suspicion was confirmed using dark field TEM, in which particles of the Laves compound 5–10 nm in diameter were imaged by placing the objective aperture on the $\langle 111 \rangle$ C15 ring, with 0.401 nm d spacing. The chemical order present in the small quantity of this phase contained in the sample is dominant, which suggests a rather small degree of chemical order in the majority bcc phase of the as-milled sample.

In order to use the present data to evaluate chemical ordering in bcc Ti-Cr, the data for the as-milled powder were subtracted from that of the annealed powder. The resulting $\Delta S(Q) = S(Q)_{\text{annealed}} - S(Q)_{\text{milled}}$ is shown as Fig. 8. While oscillations typical of CSRO are clearly recognizable in $\Delta S(Q)$, the corresponding subtracted $G(r)$'s showed a pronounced high-frequency oscillation which was inconsistent with the bcc lattice. Because this oscillation is either an artifact due to normalization errors in the $S(Q)$'s or to relaxation occurring in the residual Laves compound, the approach was adopted of fitting a modeled bcc CSRO to the measured $S(Q)$. The functions adopted were Gaussians located at the neighbor shells of the bcc lattice, using the lattice parameter determined from x-ray diffractometry. It was thus assumed that $\Delta G(r)$ should have the form

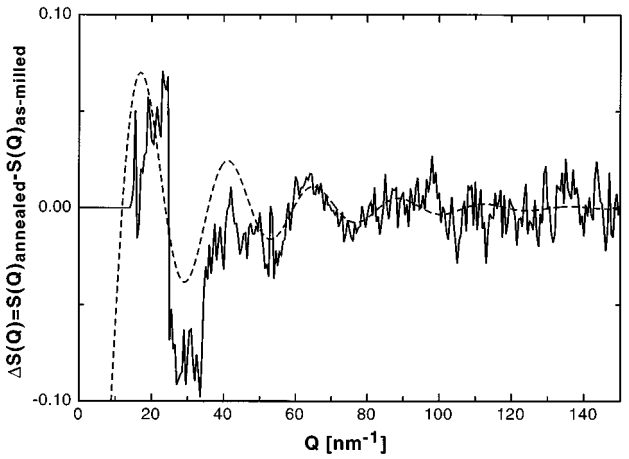

FIG. 8. Difference $\Delta S(Q)$ representing the change in $S(Q)$ induced by a brief anneal of the MM powder at 350 °C. The dashed line represents a best fit to the data assuming $\Delta G(r)$ consists of a single Gaussian peak at the first-neighbor shell, $r_1 = 0.2643$ nm.

$$\Delta G(r) = \sum_p a_p e^{-b_p^2 (r - r_p)^2} \tag{10}$$

in which a single Gaussian resides at each of the p neighbor shells of the bcc phase at $r = r_p$, and a_p and b_p are fit parameters. In this case, $\Delta S(Q)$ is given by

$$\Delta S(Q) = \frac{1}{Q} \sum_p \frac{\sqrt{\pi} a_p}{b_p} e^{-Q^2/4b_p^2} \sin Q r_p . \tag{11}$$

Unfortunately, due to a weak signal, as well as the presence of spurious discontinuities in $\Delta S(Q)$ at $Q \approx 24$ and 34 nm^{-1}, the uncertainty was too large to allow reliable fit parameters to be obtained beyond the first-neighbor shell. The resulting a_1 and b_1 are -31 ± 15 nm^{-2} and 44 ± 26 nm^{-1}, respectively, and the fit to $\Delta S(Q)$ using these parameters is shown as a dashed line in Fig. 8. As can be seen from Fig. 8, reduction of the discontinuities would result in better agreement with the modeled $\Delta S(Q)$. The data for $Q \leqslant 14$ nm^{-1} contained artifacts. It is set equal to zero in Fig. 8, and was not used in the fit. From the parameter b_1, the full width at half maximum of the Gaussian representing the first-neighbor shell is 0.038 ± 0.01 nm, between which lies more than 80% of this shell. Using Eq. (6), the change in the CSRO parameter for the first-neighbor shell, $\Delta\alpha_1$, lies between -0.024 and -0.072, with a best fit value of -0.032. This indicates a slight tendency for unlike nearest neighbors to be preferred, so that a Ti atom has on average 0.14 more Cr nearest neighbors after a brief anneal at 350 °C than after milling. The smallness of the increase of CSRO in the bcc phase is consistent with the requirement for inverse melting that the energy associated with CSRO in the bcc phase be weak. The result of a preference for unlike near neighbors in the Ti-Cr bcc phase is consistent with a previous neutron-diffraction study performed on a bulk-quenched alloy.[18] A model for electronically stabilized CSRO in Ti-based alloys which has been previously proposed based on diffuse electron scattering[28] could not be tested due to the absence of reliable values for α beyond the first-neighbor shell.

V. DISCUSSION

The neutron-diffraction characterization of inverse melted amorphous $Ti_{45}Cr_{55}$ has demonstrated that the inverse melting transformation is associated with an increase in CSRO with respect to the precursor milled bcc phase. The measurements allow specification of the type of CSRO in the amorphous phase through assessment of first-neighbor coordinations. Two central points concerning the CSRO emerge from the assessed coordinations: First, the change in local coordination from bcc to the amorphous state in inverse melting involves a differentiation of Ti and Cr sites in the material. This differentiation is implicit in the difference in Ti and Cr coordination numbers $\Delta N \approx 3$–4 which the data support. It is further shown by the existence of peak 1 in the $G(r)$ corresponding to Cr-Cr pairs. From the 0.245 nm distance of this peak, it is evident that the Cr atoms in the first-neighbor shell of Cr cannot be exchanged with Ti atoms, as the result would

deviate significantly from the expected 0.285 nm Ti-Cr bond length. The second point concerning the CSRO is that it does not significantly change the numbers of like and unlike pairs from the random case. The first-neighbor coordination shells for both Cr and Ti have about 45–56 at. % Ti. The deviation from the average concentration is thus not pronounced. This evidence of a weak ordering tendency in the classical Bragg-Williams sense is consistent with the thermodynamics of the Ti-Cr system,[1,29] which is characterized by small heats of mixing, i.e., a small enthalpy of interaction between Ti and Cr. As has been pointed out previously,[30] this is typical of systems which undergo inverse melting. The chemical ordering occurring on inverse melting, which mainly involves a differentiation of Cr and Ti sites, can account for the decrease in entropy accompanying the *c*-to-*a* transformation, as presented in the Introduction.

The neutron-diffraction results indicate a dramatic structural change in inverse melting with respect to the bcc topology of the precursor phase. In particular, similarities exist in the local structure between the amorphous phase and the $TiCr_2$ Laves compound. As was shown, the first-neighbor coordinations in the amorphous phase resemble those of the $TiCr_2$ Laves compound, and further similarity is supported by the correspondence between peaks in the $G(r)$ and those of a $TiCr_2$ $G(r)$ up to a distance $r \approx 0.7$ nm. In further support of this, modeling of the present data using the Laves phase structure has been performed,[27] and reasonable agreement was found using the Laves phase structure and a length scale for structural units of ≈ 2.5 nm. Because the Laves compound is a topologically close-packed structure, characterized by the presence of exclusively tetrahedral interstices, this is indicative of a dramatic departure from the bcc topology of the precursor phase. This supports the suggestion that the occurrence of inverse melting in an alloy depends on the energy reduction on ordering being coupled with a pronounced topological change from the precursor bcc topology.[8] The present neutron-diffraction data demonstrate that this is clearly the case, as the local structure of the amorphous phase is more close packed, and similar to that of the Laves compound. In spite of this similarity, there are significant differences between the amorphous and Laves phase local structures, as is indicated by deviations in the first-neighbor coordinations.

The present similarity between the local structure of the amorphous phase and that of the Laves compound is not an isolated case, as it has frequently been found previously that the amorphous phase local structure may resemble that of a stable compound phase with a composition near that of the amorphous alloy.[15–17,31] The significance of compoundlike local structures in the amorphous phase is further supported by recent thermodynamic characterization of early-transition-metal–late-transition-metal amorphous alloys, which has shown that the amorphous phase may possess complex Gibbs energy versus composition $[G(x)]$ dependencies, with distinct minima occurring in $G(x)$ at particular compositions.[32] The $G(x)$ minima must result from local structures which are energetically favorable at certain compositions. In the Zr-Fe and Zr-Co systems, $G(x)$ minima are found near to the $ZrFe_2$ and $ZrCo_2$ stoichiometries, which may indicate Laves-like local structures in these alloys.[32] This suggests that the similarity between the amorphous and Laves phase local structures found in the present work may be a fairly general characteristic of early-transition-metal–late-transition-metal amorphous alloys with compositions near to AB_2.

The present $S(Q)$ is distinct from previously measured $S(Q)$'s for other amorphous phases in possessing well-defined maxima up to a large Q of about 80 nm^{-1}. This feature is not shared by other null matrix $S(Q)$'s,[16,33,34] or other $S(Q)$'s for amorphous metallic phases which are not null-matrix alloys.[17,35,36] The peaks in $S(Q)$ are associated with features in $G(r)$, which are quite different from the broad oscillations in $G(r)$'s for other amorphous metal alloys. These differences are explainable based on the variability of medium-range order (MRO) within the amorphous phase. It is well known that amorphous structures may vary considerably with respect to the degree of MRO:[23,37,38] Whereas amorphous phases produced by conventional means such as melt spinning at high cooling rates may display relatively little MRO,[38] the present amorphous phase was produced by a process of thermal annealing at the relatively high temperature of 650 °C. It is therefore not surprising that the MRO is quite pronounced in the present case.

The tendency for MRO to increase with thermal treatment of amorphous phases prior to crystallization is supported by previous calorimetric investigations and results of high-resolution transmission electron microscopy (HRTEM) in metallic amorphous alloys.[23,39] In a recent HRTEM study of inverse melting in a $Nb_{45}Cr_{55}$ alloy[23] MRO domains with 2–3 nm diameters were found in amorphous cosputtered $Nb_{45}Cr_{55}$ films which were heated to the temperature at which inverse melting occurs. Both TEM images and electron-diffraction support the structural similarity of inverse melted alloys and codeposited amorphous films which have been subjected to the same heat treatment. Pronounced MRO is thus an inherent characteristic of the heat treated amorphous phase in alloys which can undergo inverse melting, regardless of whether the alloy was produced by inverse melting or another method such as codeposition. The MRO seen in the present results is due to the relatively high temperature at which inverse melted amorphous alloys are produced. Further work is needed to determine whether pronounced MRO is a general characteristic of amorphous phases which are produced at high temperatures at which atomic mobility is significant, for instance, in solid-state amorphization reactions of elemental thin films,[40] or nonpolymorphous precipitation of an amorphous phase from a supersaturated solid solution.[41]

An additional source of pronounced structure in the neutron-diffraction data may also be a small quantity of $TiCr_2$ compound which the x-ray diffraction trace suggests may be present in the alloy. Nevertheless, this quantity is small, and is estimated to be much less than 5 vol % based on a maximum x-ray peak height in Fig. 3 trace *b*) which is approximately 5% of that for a fully crystallized alloy.

VI. CONCLUSIONS

Diffuse neutron-scattering measurements on bcc and inverse melted amorphous $Ti_{45}Cr_{55}$ have shown that the transformation from bcc to the amorphous phase is associated with an increase in the CSRO. The order consists of a differentiation in the amorphous phase between Ti and Cr sites. An increase in the CSRO is consistent with the thermodynamics of inverse melting, which indicate a decrease in en-

tropy accompanying the *c*-to-*a* transformation.

The neutron-scattering results indicate similarities in the local structure between the amorphous phase and the $TiCr_2$ Laves compound, as well as an unusual degree of topological order for an amorphous phase. These structural aspects are consistent with pronounced MRO in the amorphous phase produced by inverse melting of a supersaturated solid solution, which results in a thermally relaxed amorphous structure.

ACKNOWLEDGMENTS

The authors wish to thank H.-Y. Bai, C. Gente, and T. Klassen for valuable discussions. Particular thanks also goes to A. C. Hannon for experimental assistance and critical reading of the manuscript. Funding for the project from the Deutsche Forschungsgemeinschaft DFG-SP, Unterkühlte Metallschmelzen, Az: Bo 691/5-1 is gratefully acknowledged.

*Present address: Dept. of Materials Science and Engineering, Northwestern University, 2225 Sheridan Rd, Evanston, IL 60208-3108.

[1] Z. H. Yan, T. Klassen, M. Michaelsen, M. Oehring, and R. Bormann, Phys. Rev. B **47**, 8520 (1993).
[2] C. Michaelsen, M. Oehring, and R. Bormann, Appl. Phys. Lett. **65**, 318 (1994).
[3] W. Sinkler and R. Bormann, unpublished work on the Zr-Mo system.
[4] C. Michaelsen, unpublished work on the Ta-Cr system.
[5] A. L. Greer, J. Less-Common Met. **140**, 327 (1988).
[6] R. Bormann and K. Zöltzer, Phys. Status Solidi **131**, 691 (1992).
[7] W. Sinkler, Ph.D. thesis, University of Pennsylvania, 1993.
[8] W. Sinkler, C. Michaelsen, and R. Bormann, in *Metastable Phases and Microstructures*, edited by R. Bormann, G. Mazzone, R. S. Averback, R. D. Shull, and R. F. Ziolo, MRS Symposia Proceedings No. 400 (Materials Research Society, Pittsburgh, 1996), p. 185.
[9] C. W. Allen, L. E. Rehn, and H. Wiedersich, Appl. Phys. Lett. **50**, 1876 (1987).
[10] C. W. Allen and L. E. Rehn, Ultramicroscopy **30**, 188 (1988).
[11] K. K. Larsen, Ph.D. thesis, University of Aarhus, 1993.
[12] W. Sinkler, D. E. Luzzi, and C. W. Allen, Scr. Metall. **28**, 863 (1993).
[13] W. Sinkler (unpublished).
[14] W. Sinkler and D. E. Luzzi, J. Alloys Compd. **194**, 273 (1993).
[15] R. Wang, Nature **278**, 700 (1979).
[16] T. Fukunaga, T. Kai, M. Naka, N. Watanabe, and K. Suzuki, in *Proceedings of the 4th International Conference on Rapidly Quenched Metals*, edited by T. Masumoto and K. Suzuki (Japan Institute of Metals, Sendai, Japan, 1982), p. 347.
[17] K. Suzuki, J. Phys. Condens. Matter **3**, F39 (1991).
[18] A. Blatter and W. Bührer, Mater. Sci. Eng. A **133**, 431 (1991).
[19] A. B. Bhatia and D. E. Thornton, Phys. Rev. B **2**, 3004 (1970).
[20] B. E. Warren, *X-Ray Diffraction* (Addison-Wesley, Reading, MA, 1969).
[21] C. Michaelsen, Z. H. Yan, and R. Bormann, J. Appl. Phys. **73**, 2249 (1993).
[22] E. Rudy, compilation of phase diagram data, Technical Report AFML-TR-65-2, Part V, Wright Patterson Air Force Base, Ohio (1969).
[23] W. Sinkler, C. Michaelsen, and R. Bormann, J. Mater. Res. (to be published).
[24] A. K. Soper, W. S. Howells, and A. C. Hannon, *ATLAS Version 1.0.*, Rutherford Appleton Laboratory, Chilton, U.K. (1989).
[25] A. C. Hannon, W. S. Howells, and A. K. Soper, *Second Workshop on Neutron Scattering Data Analysis* (*WONSDA*2), IOP Conf. Proc. No. 107 (Institute of Physics and Physical Society, London, 1990), p. 193.
[26] P. Duwez and J. L. Taylor, Trans. ASM **44**, 495 (1952).
[27] A. C. Hannon (private communication).
[28] W. Sinkler and D. E. Luzzi, Acta Metall. Mater. **42**, 1249 (1994).
[29] J. L. Murray, in *Phase Diagrams of Binary Titanium Alloys*, edited by J. L. Murray (ASM International, Metals Park, OH 1987), p. 68.
[30] R. Bormann, Mater. Sci. Eng. A **179/180**, 31 (1994).
[31] E. Nassif, P. Lamparter, and S̆. Steeb, Z. Naturforsch. **38a**, 1206 (1983).
[32] F. Gärtner, C. Michaelsen, and R. Bormann, Philos. Mag. B (to be published).
[33] M. Sakata, N. Cowlam, and H. A. Davies, in *Proceedings of the 4th International Conference on Rapidly Quenched Metals* (Ref. 16), p. 479.
[34] D. Spilsbury, Ph.D. thesis, University of Sheffield, 1996.
[35] P. Lamparter, S. Steeb, and E. Grallath, Z. Naturforsch. **38a**, 1210 (1983).
[36] Y. Waseda and H. S. Chen, in *Proceedings of the 3rd International Conference on Rapidly Quenched Metals*, edited by B. Cantor (The Metals Society, Sussex, England, 1978), Vol. 2, p. 415.
[37] P. H. Gaskell, D. J. Smith, C. J. D. Catto, and J. R. A. Cleaver, Nature **281**, 465 (1979).
[38] Y. Hirotsu, M. Uehara, and M. Ueno, J. Appl. Phys. **59**, 3081 (1986).
[39] K. Anazawa, Y. Hirotsu, and Y. Inoue, Acta Metall. Mater. **42**, 1997 (1994).
[40] R. B. Schwarz and W. L. Johnson, Phys. Rev. Lett. **51**, 415 (1983).
[41] H. Schlüter, H. C. Freyhardt, H. U. Krebs, and R. Bormann, Z. Phys. Chem. **157**, 407 (1988).